UTILIZING BONDED ZIRCONIA-KAOLIN COMPOSITE SYSTEM FOR CRAFTING GLASS MELTING CRUCIBLES

I. J. AKINRULI A.S. SHADO AND E. T. ALIU

Department of Glass and Ceramic Technology, School of Science and Computer Studies, The Federal Polytechnic Ado Ekiti, P.M.B 5351 Ado Ekiti, Nigeria

Corresponding author's email -shadoadeniyi@gmailauthor's.com

ABSTRACT

This study, aims to incorporate fine zircon particles into a finely-grained kaolin-zircon composite through thermal decomposition with reaction sintering. Several batches were prepared with different ratios of zircon (10%, 50%, and 90% respectively) mixed with kaolin. The preparation process involved milling the starting materials, semi-dry uniaxial pressing, and reactive sintering at a temperature of 1200°C. X-ray diffraction patterns confirmed the presence of predicted phases, namely ZrO2 and Al6Si2O13, in all the batches according to the phase diagram. The addition of a lower amount of zircon to kaolin led to reduced porosity and improved bulk density of the kaolin-zircon composite. Furthermore, it enhanced the composite's resistance to thermal shock. Increasing the amount of zircon particles in the kaolin matrix resulted in improved mechanical properties due to the phase transformation of zircon from tetragonal to monoclinic phase. Micro-hardness also increased with higher zircon content, with hardness values of 79.8HV, 87.3HV, and 91.2HV for composite samples S1, S5, and S9, respectively. To assess corrosion, tests by immersing the kaolin-zircon composites into molten glass at a temperature simulating actual service conditions. It was found that the extent of corrosion decreased with higher refractory zircon content and increased with increasing porosity. Wetting of the composite by the glass decreased with increasing zircon content. Conclusively, porosity and wettability were significant factors influencing the composite's susceptibility to glass penetration and, consequently, controlling the rate of corrosion. Microstructural examination using SEM revealed that the zirconia derived from the zircon appeared to be less reactive towards the molten glass in the interfacial zone.

Keywords: composite, mechanical properties, Corrosion, Porosity, wettability

1. INTRODUCTION

All through history of the ceramic industries, different types of materials or compositions have been utilized due to some specific benefit, inherent property such as superior strength, lower electrical conductivity, or many other properties that could be the elementary concern for a specific application. However, excellent resistance to attack by the environment always plays a role and may, in some cases, be the prime reason for the selection of a particular material. This is especially true for those materials selected for furnace construction in the metal and glass industries. Almost all environments are corrosive to some extent. For practical applications, it comes down to a matter of kinetics—how long will a material last in a particular environment? The proper selection of materials and good design practices can greatly reduce the cost caused by corrosion. Corrosion can be considered as the debonding and subsequent physical fragmentation of the refractory, due to destruction of the bond phase by the liquid glass, together with the chemical dissolution of all phases. Attack of the sintered fine particles, and the intergranular glass-bonding phase, will be both faster, and more critical for structural integrity. In particular, the intergranular silicate glass will be susceptible to reactions with contacting molten glass. The larger grains of alumina and mullite will be attacked relatively slowly, because their specific surface areas are small. Factors determining the reactivity and solubility of the matrix phase are likely to be the accessible porosity of the refractory, which allows penetration by the corroding liquid, and the ability of this liquid to wet the refractory surfaces. Results from various studies show that the principal genesis of corrosion is related to the wetting, penetration, and reaction of molten glass with the refractory. Alkali vapours are extremely reactive and cause detrimental corrosion and control the lifetime of the refractories (Beerkens and Verheijen, 2005; Kennedy, 1981; Kashcheev et. al. 1975). One of the most severe chemical attacks on refractories

in glass melting furnaces results from alkali vapours. Zircon ($ZrSiO_4$) is commonly incorporated as a fine powder in alumina-mullite refractories to increase resistance to corrosion by molten glass. Today, researchers are focusing on a new generation of refractories, in order to decrease the infiltration and attack from molten glass. Studies have shown that reaction sintering of $ZrSiO_4/Al_2O_3$ mixture improves densification, provides better distribution of ZrO_2 particles and better fracture toughness values Lathabai, et. al. (1996); Koyama, et. al (1994); Prochazka, et. al. (1983);Anseau, et. al. (1983); Clausen, (1980); Zhao et. al. (2003). In this study the interaction between zircon powder and kaolinite clay will be examined for the development of corrosion resistant ceramic body.

In this work salient properties of kaolin-zircon system were assessed in the light of its applicability for making glass-melting crucible.

RESEARCH METHODOLOGY

Starting Materials

The starting materials (kaolin and zircon); Kaolin was collected from Okpella in Edo State, located in the Eastern extension of Igarra schist belt, in the Southwestern Nigerian basement complex which serves as a source for both alumina and silica while Zircon $Zr(SiO_4)$ was sourced from Jos, Plateau state. These materials were used for the preparation of kaolin-zircon composite.

Variables for Evaluation

In the course of this experiment the following parameters will be varied

(a). Zircon

(b). Kaolin

Line blend system will be used because it is the most valuable system for finding out simply and quickly what the response is between the two materials.

Table 1: Designation of samples in gram (g) weight fractions

Designation	Kaolinite Clay mix (%)	Zircon (%)
S_1	90	10
S_5	50	50
S_9	10	90

Table 2 - Starting materials used for the synthesis of kaolin-zircon composite.

Material	Source	Purity (%)	Particle size (μm)
Kaolin	Okpella	97.0	6.35
Zircon	Jos	98.0	2.71

Table 3 – Line blend composition of Starting materials for kaolin-zircon composite.

Zircon	10	50	90
Kaolin	90	50	10

Experimental Procedures

3.4 Preparation of Kaolin-zircon composite samples:

The kaolin and zircon were milled and homogenized by ball milling for 2 hours to increase the surface area. The milling process was done using corundum balls and distilled water as a medium, and then the powders were dried in an oven at 110 °C for 4 hours (Saud et. al. 2018). The relative amounts of the kaolin and zircon were blended using line blending of various contents of zirconia (10, 50, and 90 wt%) were added. The starting materials were mixed manually using pestle and mortar for 5 minutes. The mixed powder of the starting materials was formed in a hollow metal mold by semi-dry pressing using a uniaxial pressure. The formed sample with cylinder shape was removed from the mold and dried in a microwave oven at 110 °C for 4 minutes. Then the composite samples were sintered at in a microwave oven at 1100^{o}C.

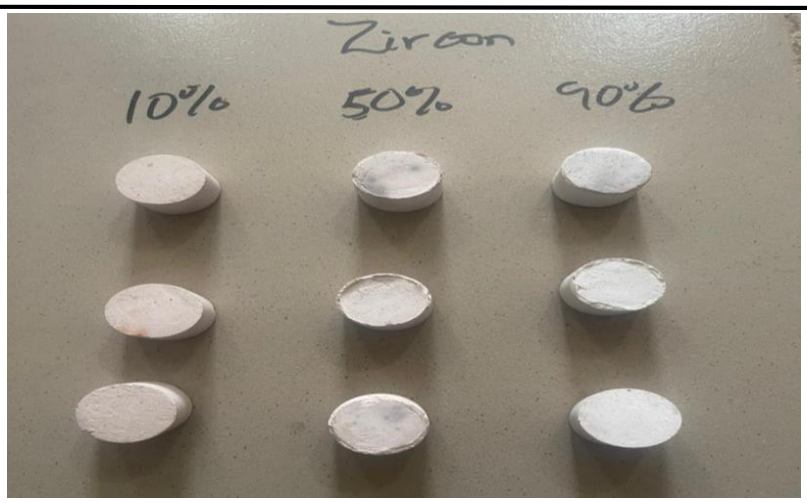

Figure 1: fired samples of kaolin-zircon composite

Characterization of Kaolin-zircon composite

***Physical properties*:** The shrinkage of kaolin-zirconia composite was due to the sintering temperature, which was measured according to the American Society for Testing and Materials (ASTM). The porosity has a significant impact on the final properties of the sintered kaolin-zirconia composite. Prepared sintered samples showed porous bodies, where the porosity was a measure of the open and closed pores. The amount of water absorbed by the body is a function of the open porosity. The water absorption represents the relationship between the mass of water absorbed in the pores to the mass of the solid part of the body. ASTM standard (C373-88) was used for measuring the bulk density, apparent porosity, and water absorption of the prepared samples; for each sample, three specimens were measured using a digital balance. The samples were dried in a microwave oven at 210 ºC for 5 minutes and then allowed for cooling down to room temperature; then, the dry weight of the kaolin-zirconia samples was measured.

Thermal properties: Thermal shock resistance was measured by heating the sample in an electric furnace at different temperatures (200, 400, and 600 °C) with a soaking time of 1 h. Then the samples were quenched in water for measuring the thermal shock resistance of the sample.

XRD analysis: Phase compositions was identified by X-ray diffraction (XRD) using an INEL CPS 120 equipment with a curved detector with a CuKa radiation (l50.154 nm) and an Ni filter, working voltage 40 kV, and working current 30 mA. The diffractograms was obtained on powder (starting materials) or on milled (fired samples) samples after 30 min as a setting time.

Chemical composition: The chemical compositions of the kaolinite clay, previously dried at 100^{o}C, was determined by XRS-FP Analysis

Thermal analysis: The starting materials were characterized by Perkin Elma thermal analysis (DTA/TGA) during heating from ambient temperature of 30^{o}C to 950^{o}C at a heating rate of 10^{o}C/min in air. The mass of the analyzed samples, previously dried at 100^{o}C, will be about 80mg.

Surface Morphology: The microstructure of fired samples was observed on polished cross sections using a scanning electron microscope (Phenom Prox Scanning Electron Microscope), working voltage 30 kV. Before observation and EDAX analyses, the samples was coated with platinum.

Water Absorption and Bulk Density Test of Tiles (Is-13630):

The tiles samples were dried in the oven at 110±5^{0}C, until it attains constant mass, i.e. when the difference between two successive weighing at intervals of 24 hours is less than 0.1%. The tile samples were cooled in the desiccators over silica gel, until cooled to room temperature. Each tile specimen was weighed and recorded as $\mathbf{M_1}$. The tiles were placed vertically, with no contact between them, in water in the water bath so that there is a depth of 50 mm water above and below the tiles. The water level 50mm was maintained above the tiles throughout the test. The water was heated until boiling and it was boiled for 2 hours. After 2 hours, the source of heat was

switched off and the tiles were allowed to cool, still completely immersed in the water, overnight. The tiles were removed from the water bath and surface water was removed from the tiles specimen by dry paper towel. Each of the tiles were immediately weighed and recorded as $\mathbf{M_2}$. The specimens were each suspended in air and were immersed in water to determine the suspended weight of each specimen $\mathbf{M_s}$.

To calculate Water absorption (%) = $[(\mathbf{M_2} - \mathbf{M_1}) / \mathbf{M_1}] \times 100$ Eqn (1)

Where, $\mathbf{M_1}$ = mass of the dry tile, in g $\mathbf{M_2}$ = mass of the wet tile, in g

Bulk density (B), in g/cm^3, of a specimen is the ratio of its dry mass divided by the exterior volume, including pores.

To calculate bulk density of tile is as follow.

$B = \mathbf{M_1} / V$ Eqn (2)

Where, B = bulk density of tile, g/cm^3

$\mathbf{M_1}$ = mass of dry tile, g

V = exterior volume, in cm^3: = $(\mathbf{M_2} - \mathbf{M_s})$

$\mathbf{M_2}$ = mass of the wet tile, in g

$\mathbf{M_s}$ = mass of suspended tile impregnated by boiling water method, in g

Apparent Porosity

The apparent porosity of the tile specimen was calculated using the formula;

Apparent porosity = $(\mathbf{M_2} - \mathbf{M_1}) / (\mathbf{M_2} - \mathbf{M_s}) \times 100$ Eqn (3)

Where, $\mathbf{M_1}$ = mass of dry tile, g. $\mathbf{M_2}$ = mass of the wet tile, in g. $\mathbf{M_s}$ = mass of suspended tile impregnated by boiling water method, in g

Percentage weight loss after firing was determined using the formula below;

% Wt. loss = $\mathbf{M_1} - M_f / \mathbf{M_1} \times \mathbf{100}$ Eqn (4)

Where, $\mathbf{M_1}$ = mass of dry tile, g. M_f = weight after firing

Dry and Fired Shrinkage

The samples were air-dried for 24 hours and oven dried at 100℃ for another 24 hours. The length at this stage was taken and was recorded as dry length. The samples were then fired at varied temperatures of 900, 1000 and 1100 respectively for 6 hours. The samples were cooled to room temperature and the fired length recorded. The dry linear shrinkage and fired linear shrinkage were calculated using the Equations (5) and (6).

% Dried shrinkage = $\mathbf{M_1} - M_2 / M_2 \times \mathbf{100}$ Eqn (5)

Where, $\mathbf{M_1}$ = mass of dry tile, g. $\mathbf{M_2}$ = mass of the wet tile, in g.

% fired shrinkage = $\mathbf{M_1} - M_f / M_f \times \mathbf{100}$ Eqn (6)

Where, $\mathbf{M_1}$ = mass of dry tile, g. M_f = weight after firing

RESULTS AND DISCUSSION

RESULTS

The chemical composition of Okpella kaolin and Zircon is shown in Table 4 and 5 while phase composition of raw kaolin and Zircon powder are shown in table 6. The starting materials and Kaolin-zircon composite were characterized by X-ray diffraction (XRD) using a diffractometer at room temperature using CuKα radiation (λ=1.5405 Å), a scanning speed of 6 °/min from 10° to 80° of 2θ, and applied power of 40 kV/30 mA. XRD patterns of the starting materials for Okpella kaolin and zircon are shown in Figure 2 and 3. respectively. Physical properties of the kaolin-zircon composite samples are shown in (Table 7). The Vickers hardness of the kaolin-zirconia composite varied with the zircon content due to the variation in porosity. The Vickers hardness of the kaolin-zircon was 10.9 GPa (90% zircon) due to the homogeneous grain size distribution. The hardness achieved the highest value with 10% zircon at 43.6 GPa due to zircon playing a significant role in the toughening of the kaolin-zircon composite system by phase transformation in the partially stabilized zircon from tetragonal to monoclinic phase that caused a change in volume in the zircon grain. Densification was improved by increasing the sintering temperature, and compaction was enhanced by increasing the amount of zircon. The decrease in the hardness value with zircon additions above 10% appears to be due to the increase in porosity, or the hardness values were measured in regions containing pores. In general, the hardness of kaolin-composite materials was affected by the crystal size, porosity, and microstructure of kaolin-zircon composite, Xiao et. al, (2020).

Table 4: Chemical composition of raw Okpella kaolin powder (%mass)

SiO_2	Al_2O_3	Fe_2O_3	CaO	TiO_2	K_2O	ZrO_2
50.86	40.64	1.50	1.69	3.48	0.32	0.27

Table 5: Chemical composition of raw Zircon powder (%mass)

SiO_2	Al_2O_3	Fe_2O_3	CaO	TiO_2	K_2O	ZrO_2
40.87	6.89	1.79	0.60	2.40	0.20	43.49

Table 6: Mineral phase composition of raw kaolin and Zircon powder

Kaolin mineral phase	Zircon mineral phase
Kaolin - $Al_2Si_2O_5(OH)_4$	Zircon – $Zr(SiO_2)$
Quartz - SiO_2	Quartz - SiO_2
Nacrite – $Al_2Si_2O_5(OH)_4$	Vermiculite - $22MgO.5Al_2O_3.Fe_2O_{3....s}$
Sepiolite – $2MgO.3SiO_2.H_2O$	Nacrite- $Al_2Si_2O_5(OH)_4$
Illite – $K(AlFe)2AlSi_3O_{10}(OH…$	Rutile – TiO_2
Clinochlore – Al-Fe- SiO_2-OH	Osumillite - K-Na-Ca-Mg-Fe-Al-S…
Garnet – 3(Ca,Fe,Mg)O.(Al,Fe…	Garnet - 3(Ca,Fe,Mg)O.(Al,Fe…

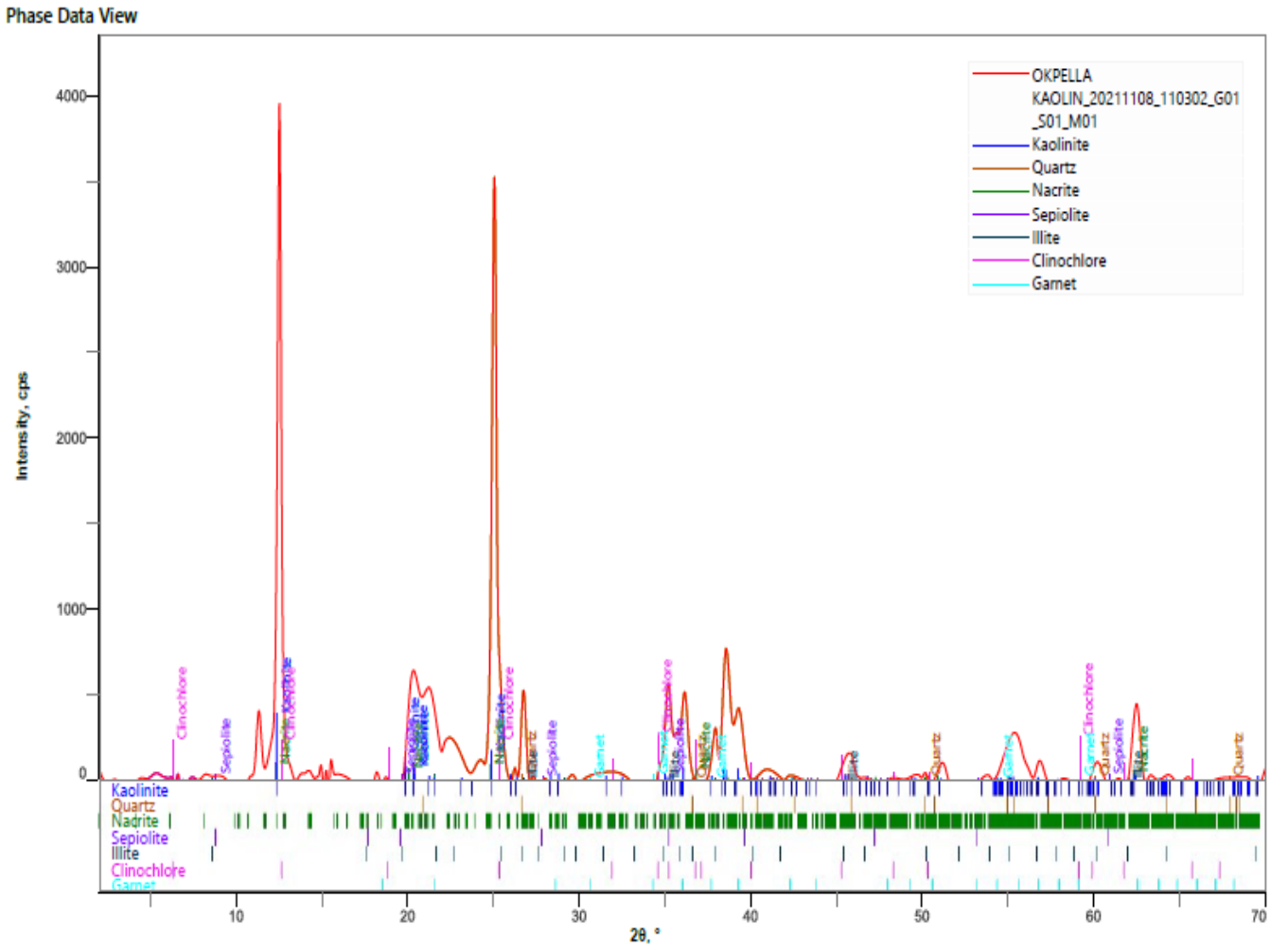

Figure 2: X-ray diffraction patterns of phase view of Okpella kaolin

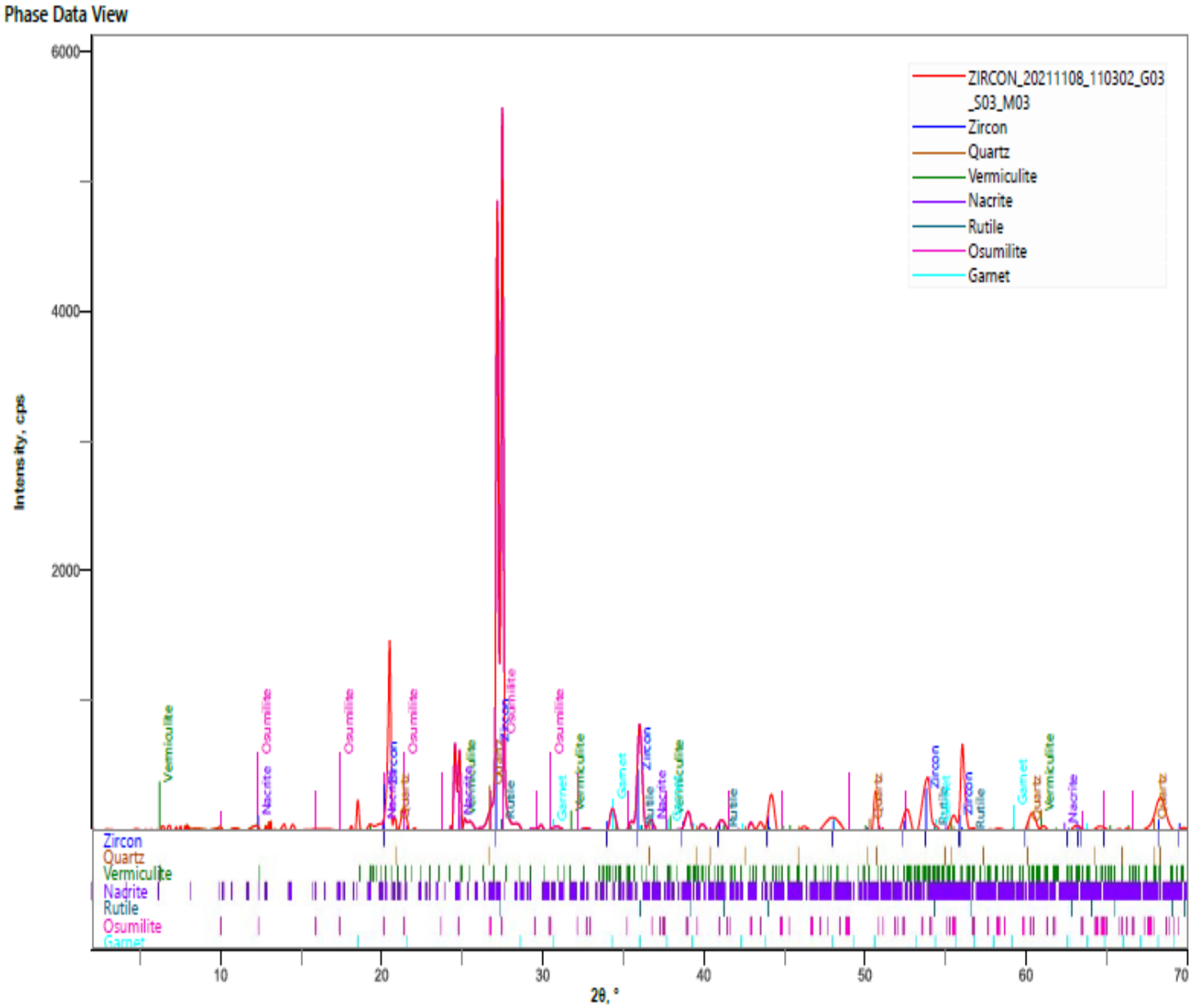

Figure 3: X-ray diffraction patterns of phase view of Zircon

Table 7: Physical properties of kaolin-zircon composite samples

Sample	S_1	S_5	S_9
Dry wt. (M_1)	28.8	28.7	28.6
Fired wt. (M_f)	25.3	26.6	27.7
Suspended wt. in air (M_s)	9.4	8.7	8.4
Porosity	7.2	7.0	12.2
Bulk Density	1.4	1.3	1.2
Water absorption	5.2	5.2	9.8
% fired shrinkage	5.0	5.0	9.0
% dry shrinkage	14	7.9	3.2
Micro hardness (VHV)	79.8	87.3	91.2

Thermal Evolution

The differential thermal analysis (DTA) indicates the steps of weight loss produced by exothermic and endothermic events. Figure 4 - 6 corresponds to DTA–TGA curves typical of kaolinite thermal evolution. The first unmarked peak corresponds to an endothermic event between 30ºC to 950ºC, correlated with a small weight loss (about Zircon content of 10, 50 and 90wt % respectively) in the TG curve, attributed to the decomposition of poorly crystalized fine-grained aluminum hydroxide Garcia-Valles et. al, (2015); Smykatz and Di, (1974); Todor, (2020). The second endothermic peak is at ~569ºC,

associated with the main weight loss in the TG. This is related to the composition dihydroxylation, loss of OH groups and to a transition phase from quartz to quartz, which implies a change in volume. Finally, an exothermic event associated with the processes of mullitization appears at about 945ºC, related to the formation of the Al_2O_3 spinel-type phase at the kaolinite–meta-kaolinite mullite transformation Brindley and Nakahira, (1959). At this temperature, the loss of weight is insignificant. Usually, the total mass loss at 1100ºC ranges from 3.1 to 12.2 wt %, depending on the clay minerals content.

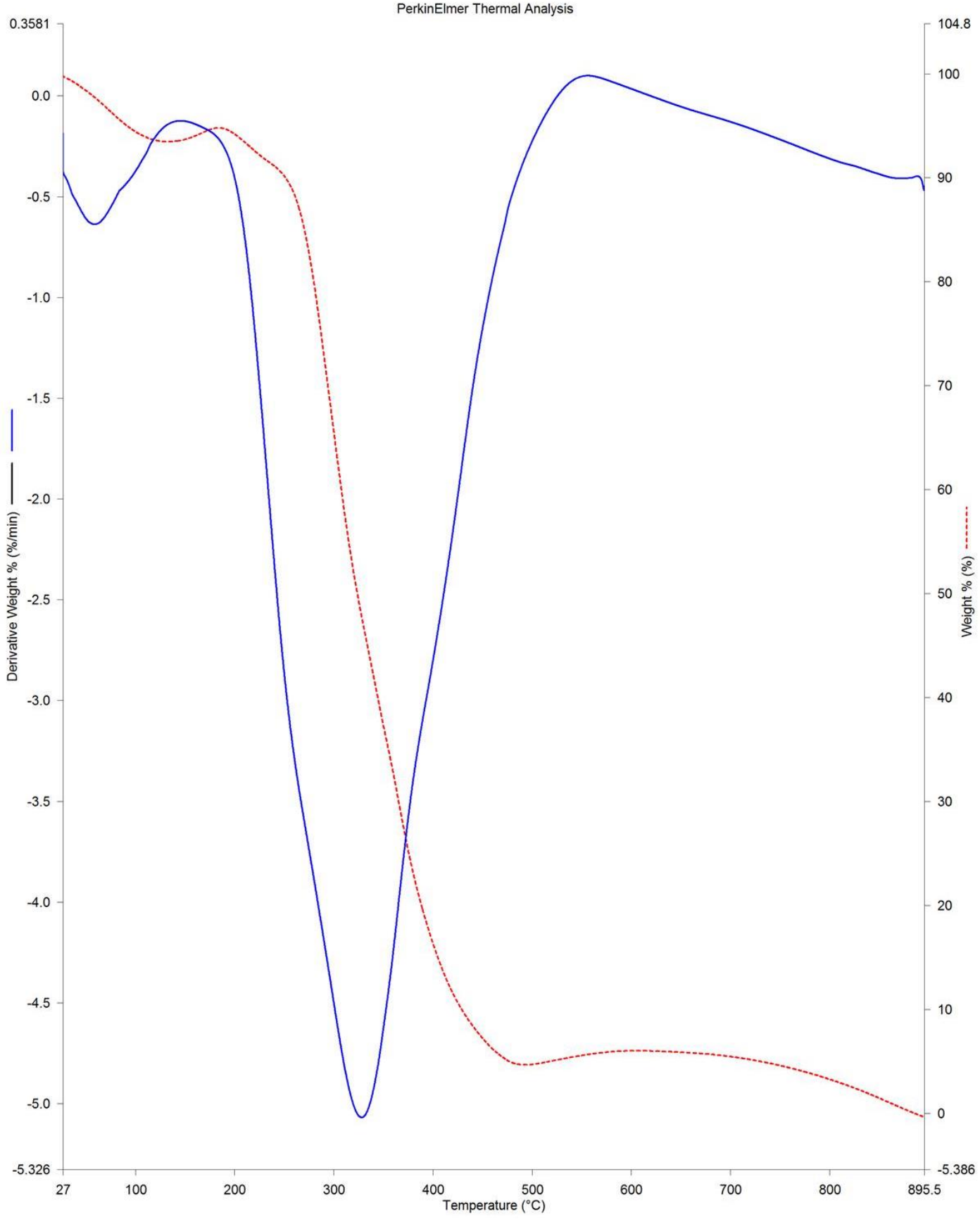

Figure 4.: TGA/DTA curve of Sample S_1 kaolin-zircon composite

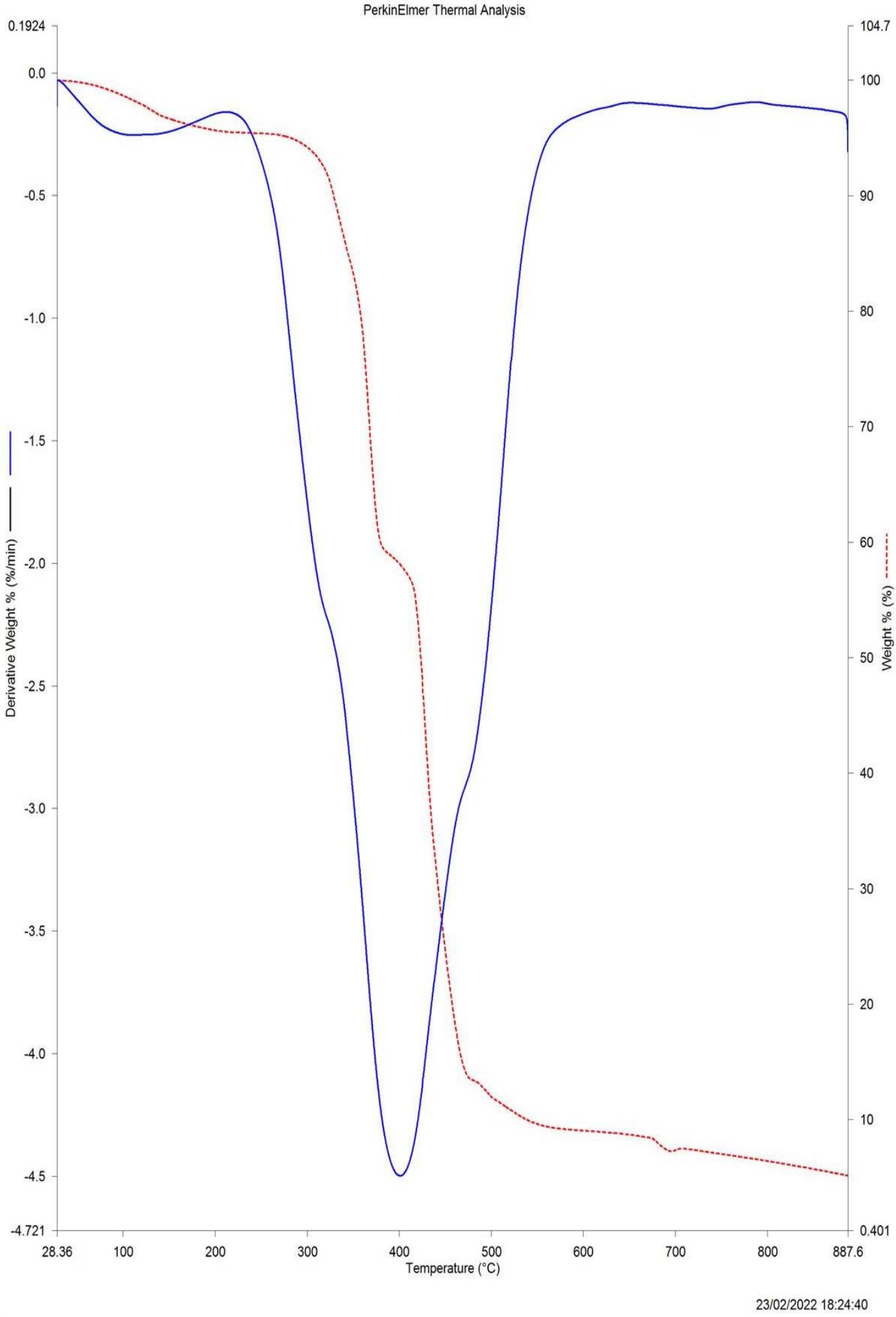

Figure 5: TGA/DTA curve of Sample S_5 kaolin-zircon composite

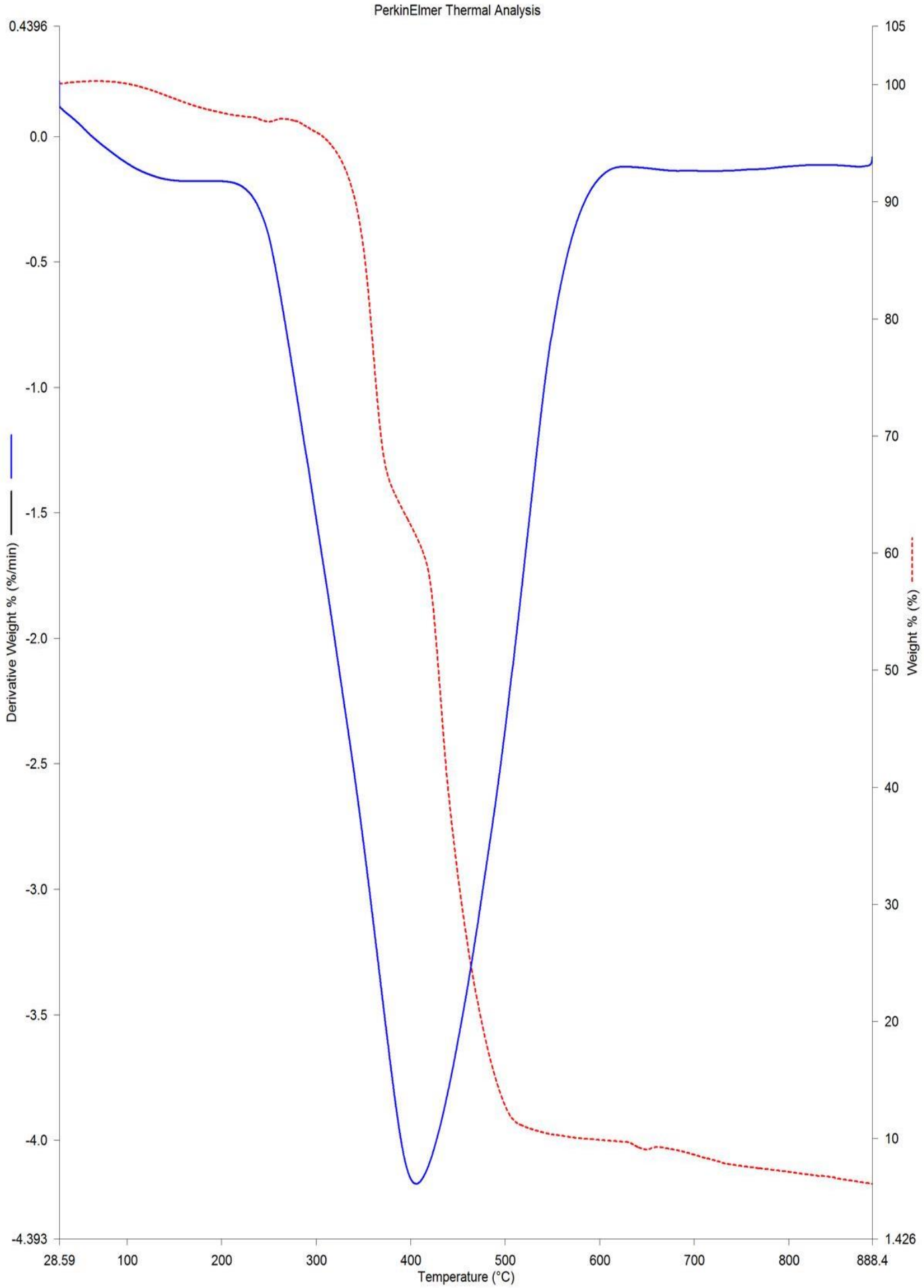

Figure 6: TGA/DTA curve of Sample S_9 kaolin-zircon composite

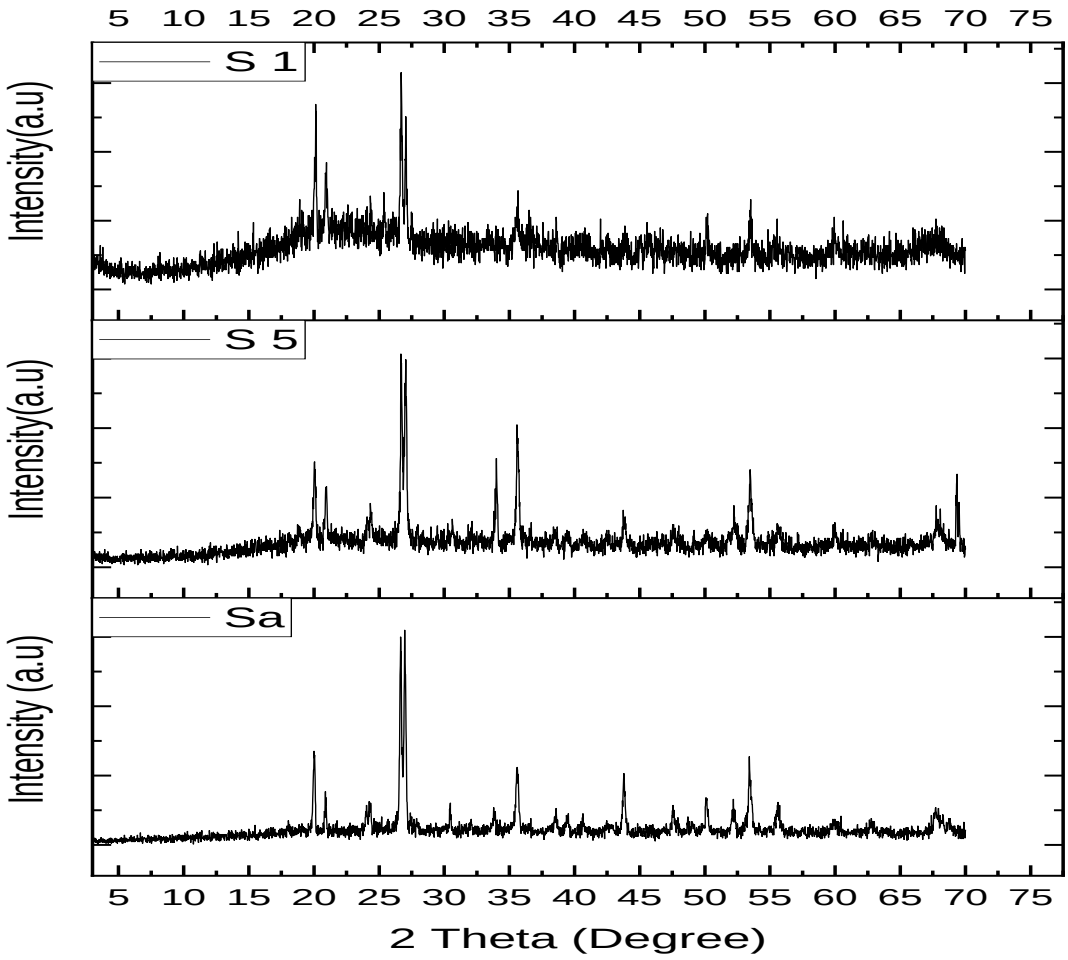

Figure 7: Super imposed graph of XRD spectra of samples S_1 S_5 and S_9

Infra-red analysis

The FTIR spectrum of the kaolin-zircon system are shown in Figure 8 - 10. The absorption bands stationed at 3,402 and 1,640 cm^{-1} correlate proportionately to expanding vibrations of water molecules while those at 998 and 788 cm^{-1} suggest the vibration of Si-O-Al group of the structure. The bands at 909 and at 789 cm^{-1} illustrate the developing vibration of Al-OH with Al in VI coordination. The band at 525 cm^{-1} suggests the vibration of Si-O-Si and Si-O-Al groups of the network (Kakali et al. 2001 and Bich et al. 2009).

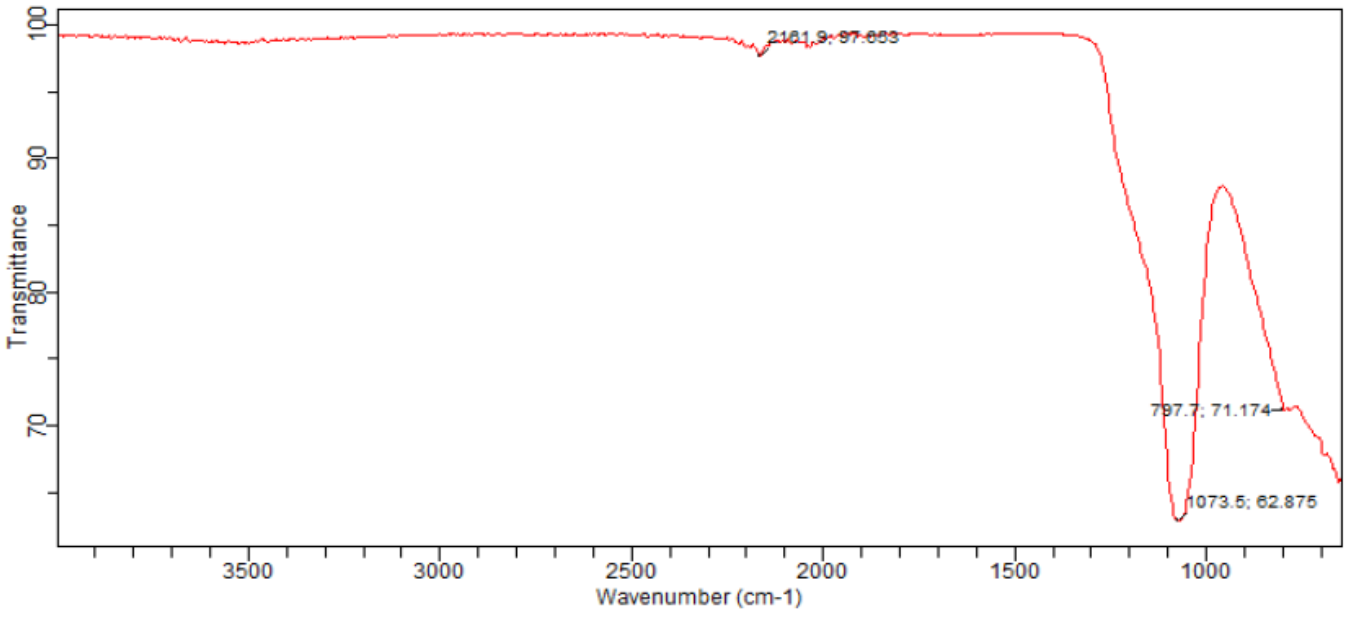

Figure 8: FTIR spectra of Sample S_1

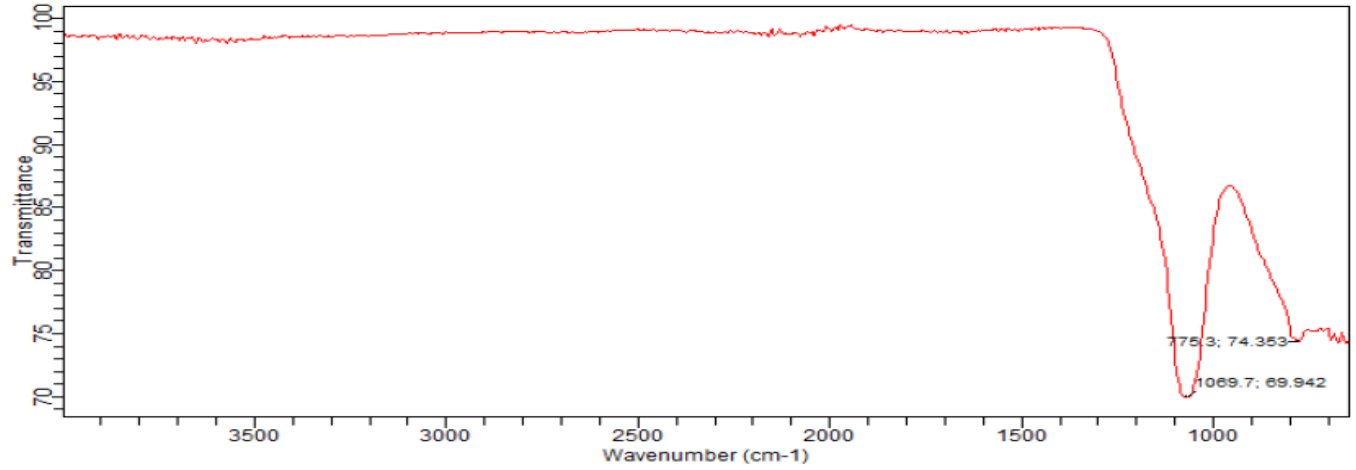

Figure 9: FTIR spectra of Sample S_5

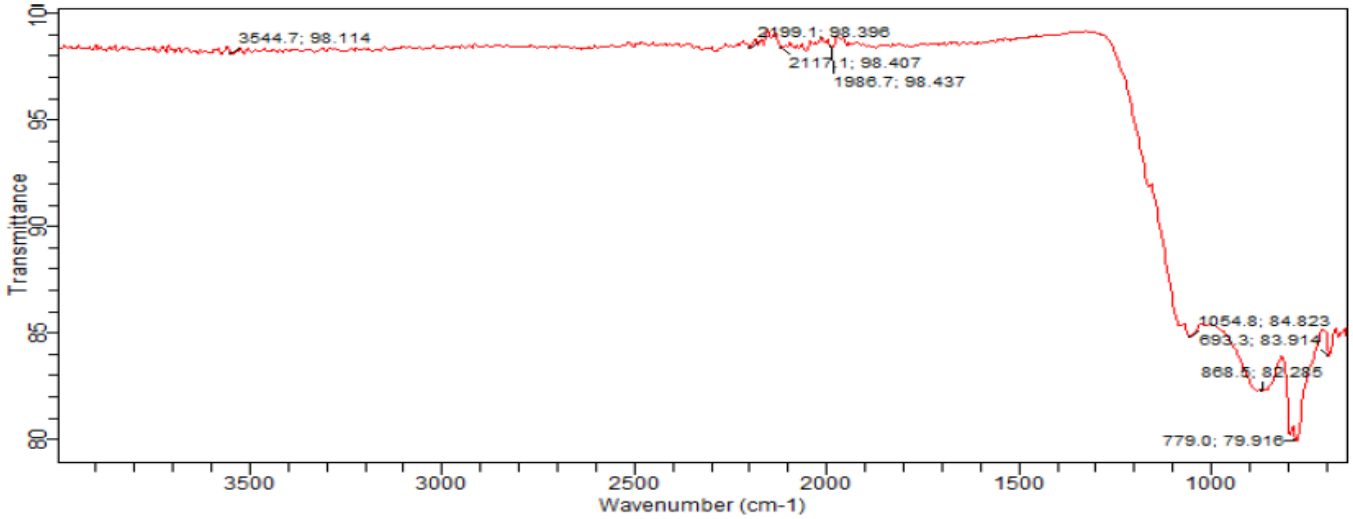

Figure 10: FTIR spectra of Sample S_9

The crystalline phases detected in the kaolin-zircon composite samples via XRD are shown in Figures 7. The alternative minerals present in Sample S_1 are Quartz (46%), Zircon (21%), Muscovite (4%) and Garnet (15.8%) with 10% zircon content. Calculation using X-ray diffraction along with chemical analysis enabled to get the quantitative mineralogical composition of composite as presented. in figure 11 to 13.

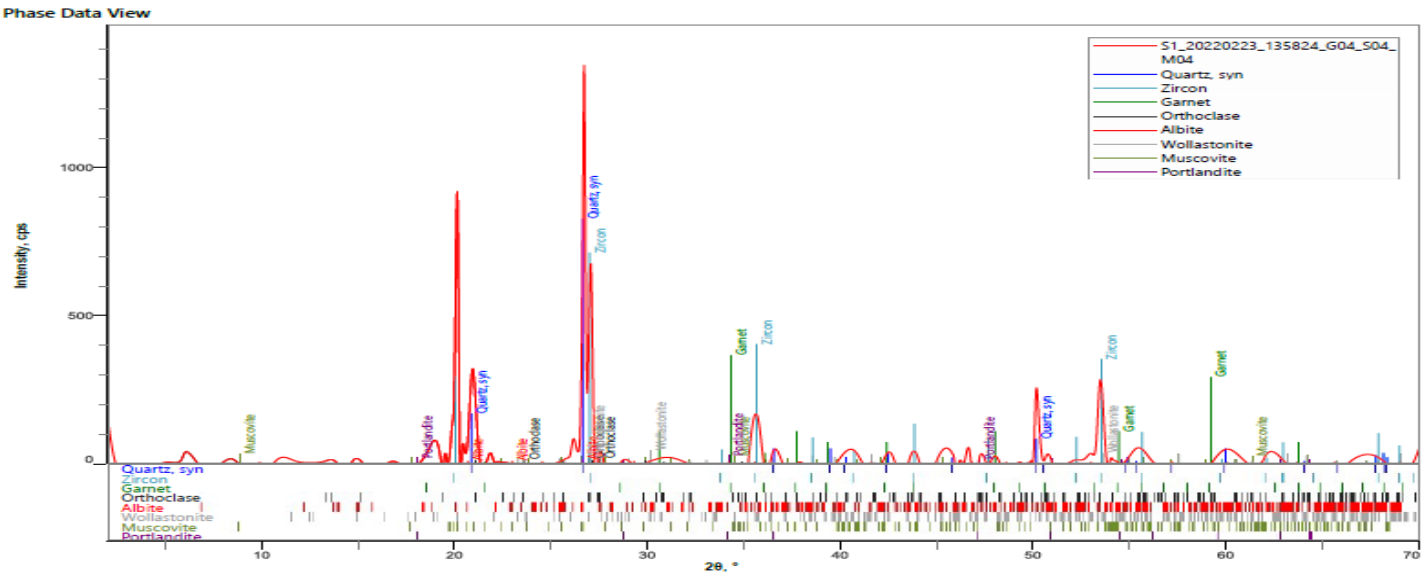

Figure 11: Phase spectrums of Sample S_1

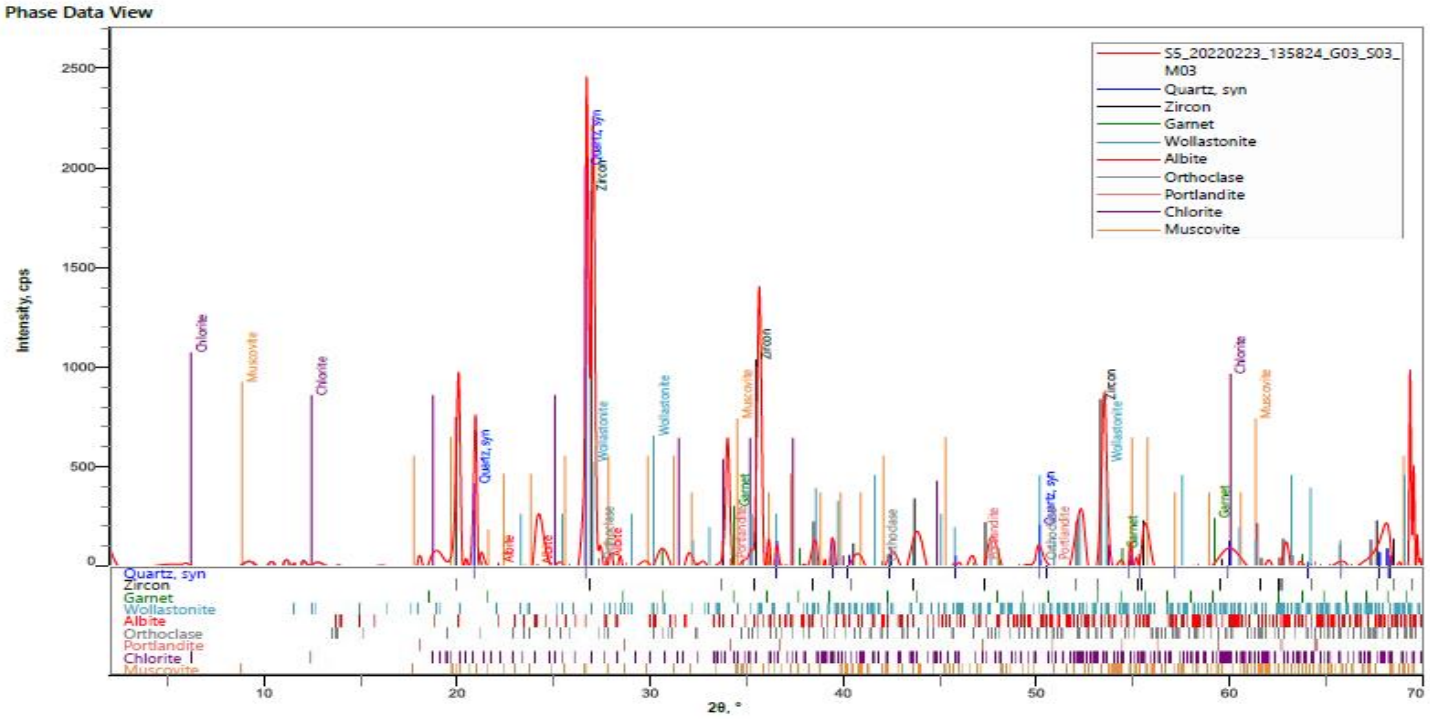

Figure 12: Phase spectrums of Sample S_5

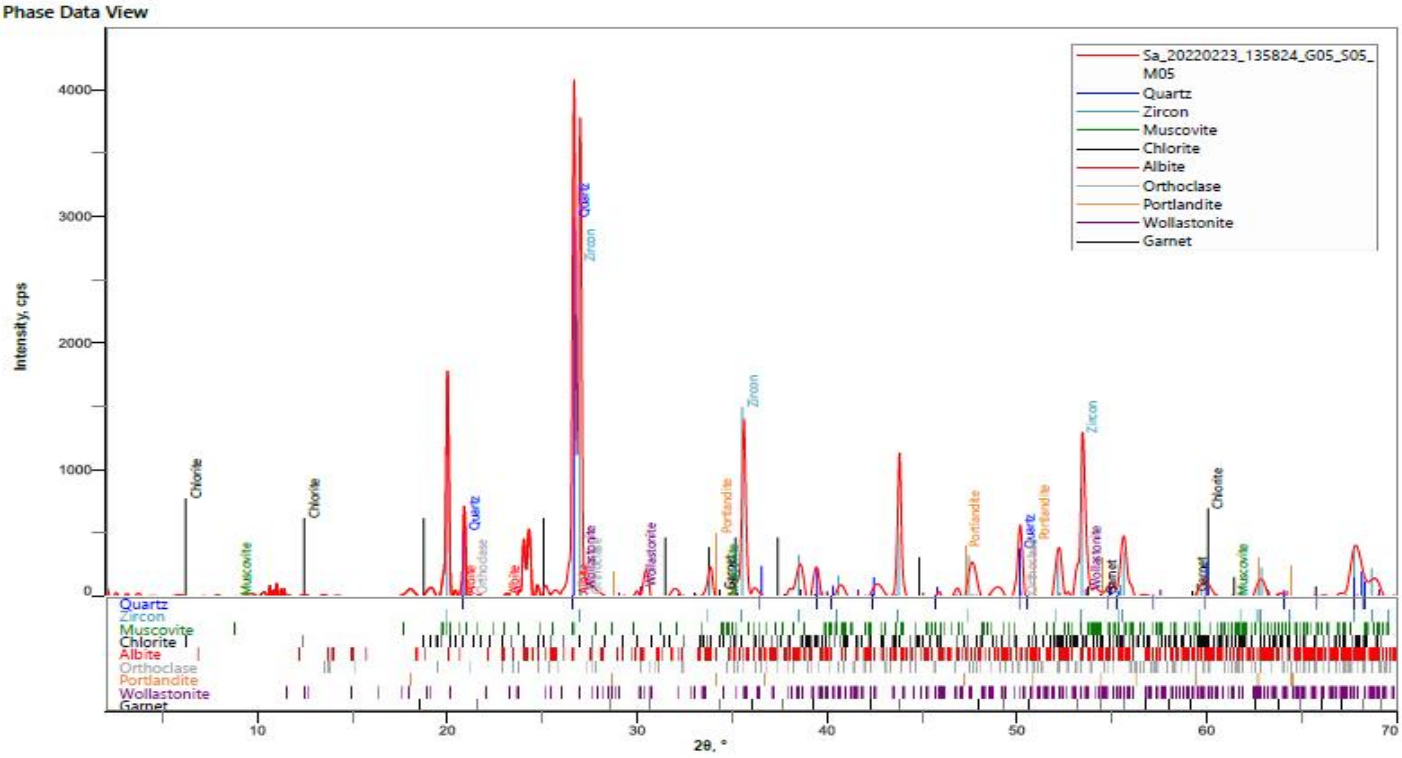

Figure 13: Phase spectrums of Sample S_9

Morphological Analysis

A SEM fitted with an EDAX analysis was used to identify minerals and study their morphology changes at temperatures of 1100ºC in kaolin-zircon composite with 10, 50 and 90% zircon contents respectively. The morphological structures are shown in Figures 14 to16. The SEM can solve the problem of determining the morphology of kaolin-zircon composite. SEM image is a highly magnified view of kaolin-zircon composite sample of S_1 shows the sample have the same main crystalline phases, such as quartz, zircon and garnet, their frequency depending largely on the base composition and crystallization parameters. It can be noticed that, with increasing the ZrO_2 content, the intensity of quartz becomes stronger at 50% zircon content.

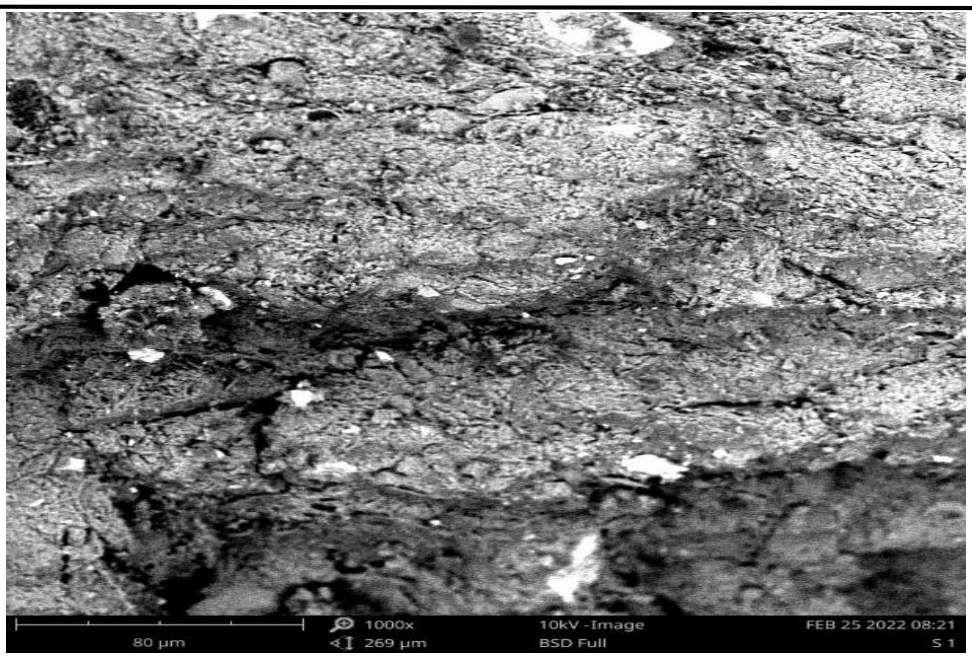

Figure 14: SEM micrograph image of Sample S_1

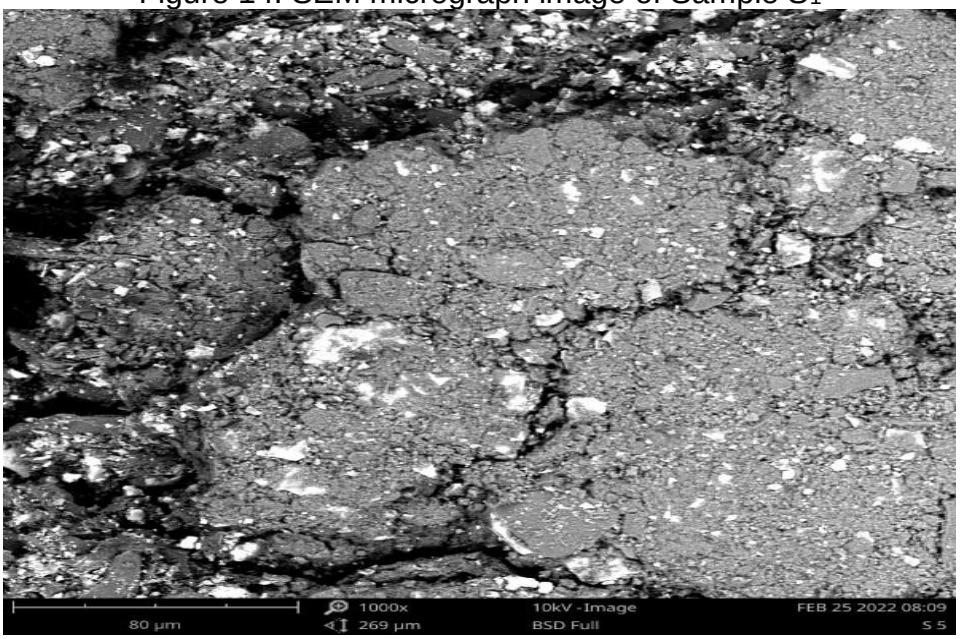

Figure 15: SEM micrograph image of Sample S_5

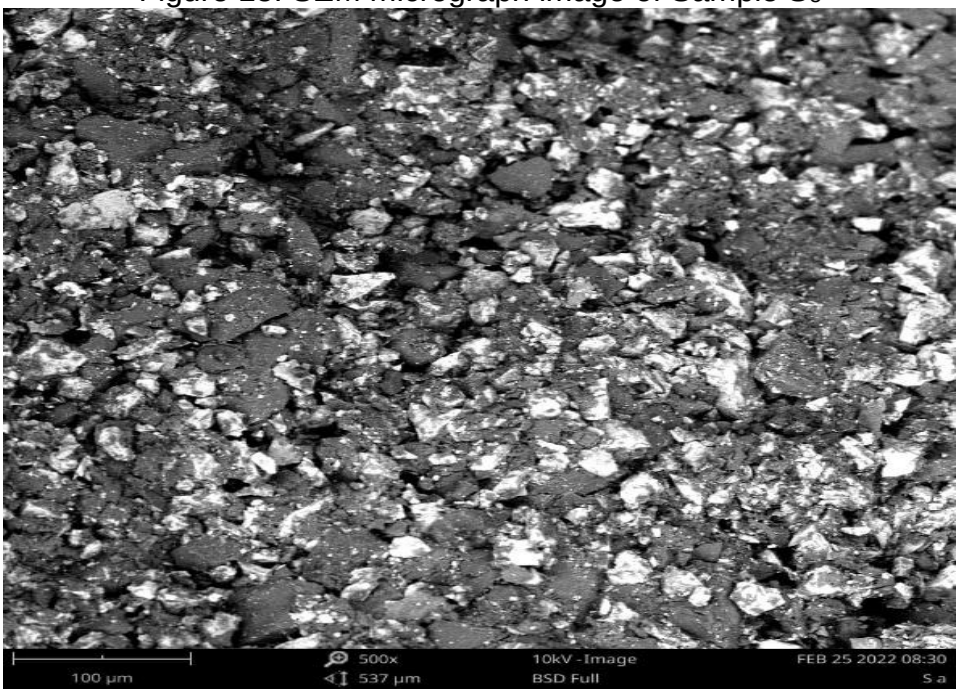

Figure 16: SEM micrograph image of Sample S_9

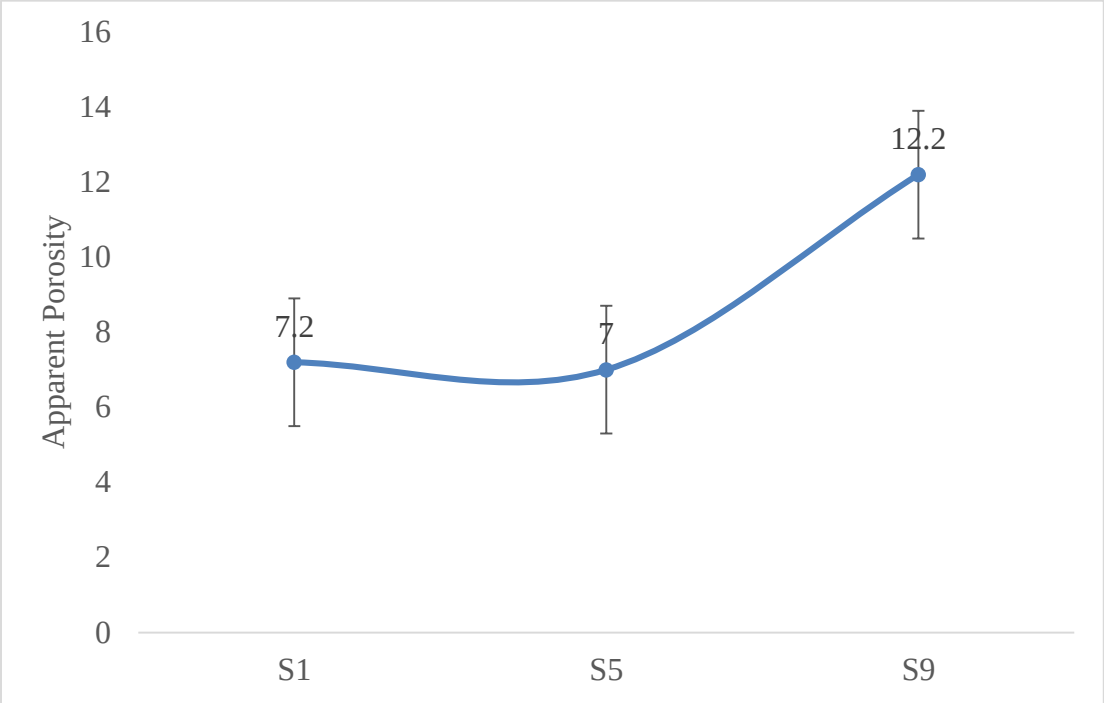

Figure 17: kaolin-zircon apparent porosity

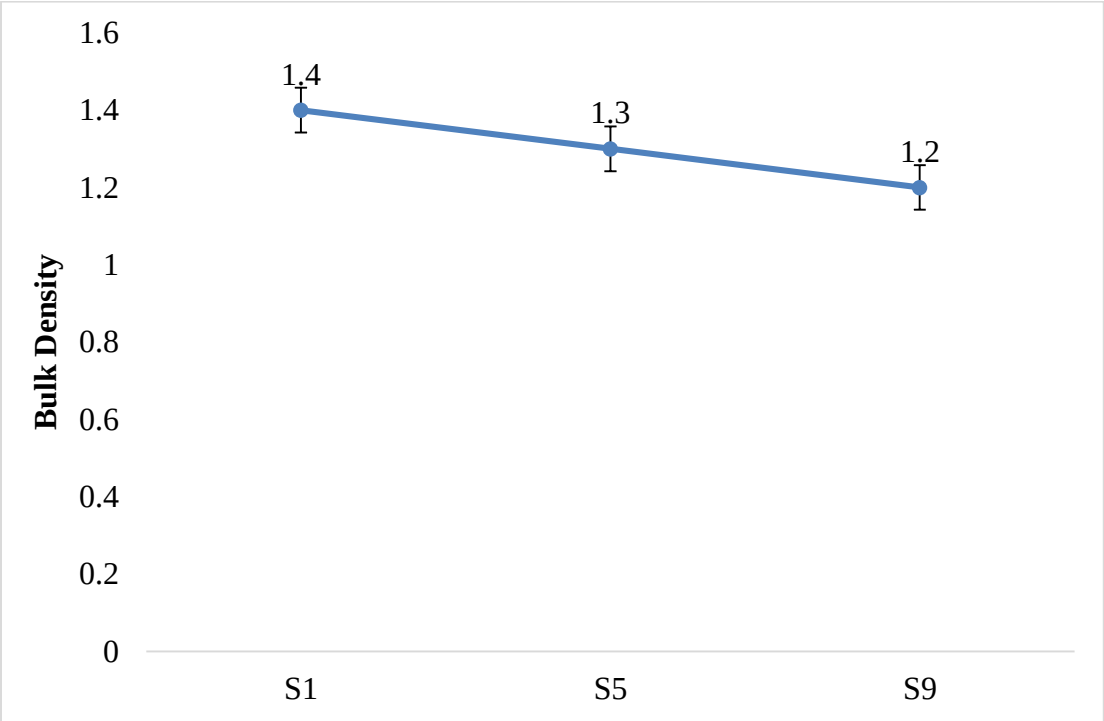

Figure 18: kaolin-zircon bulk density

The results of the physical properties of kaolin-zircon system composite are shown in Figure 17 - 20. The sintering temperature of kaolin-zircon system composite is 1100°C caused a decrease in the bulk density and increase in porosity as zircon content increases.

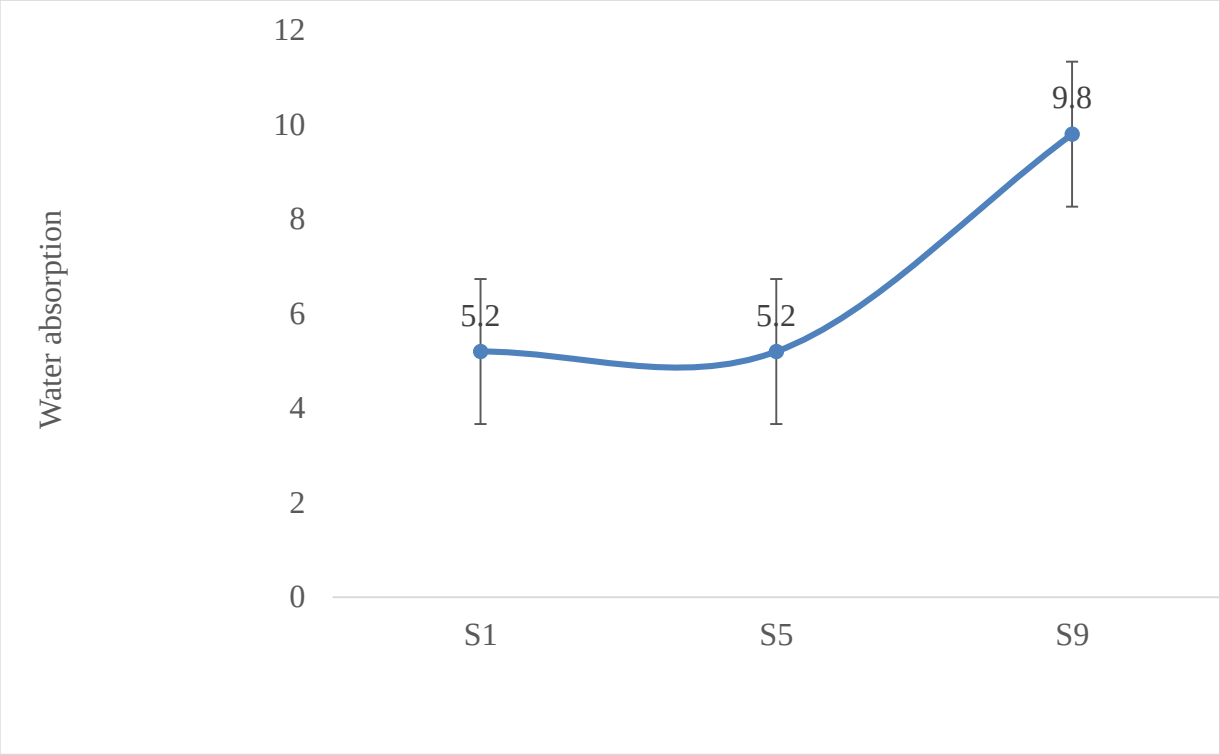

Figure 19: kaolin-zircon water absorption

The increase of porosity with the increase of the ZrO_2 content is shown in Fig. 17. This process increases the efficiency of new composites in applications to obtain a material with physical properties for porous ceramics membrane application. The apparent porosity of the composite material was 7.2% at 10% zircon content, the water absorption was 5.2%, and the lowest absorption was with the addition of 10% and 50% ZrO_2 content.

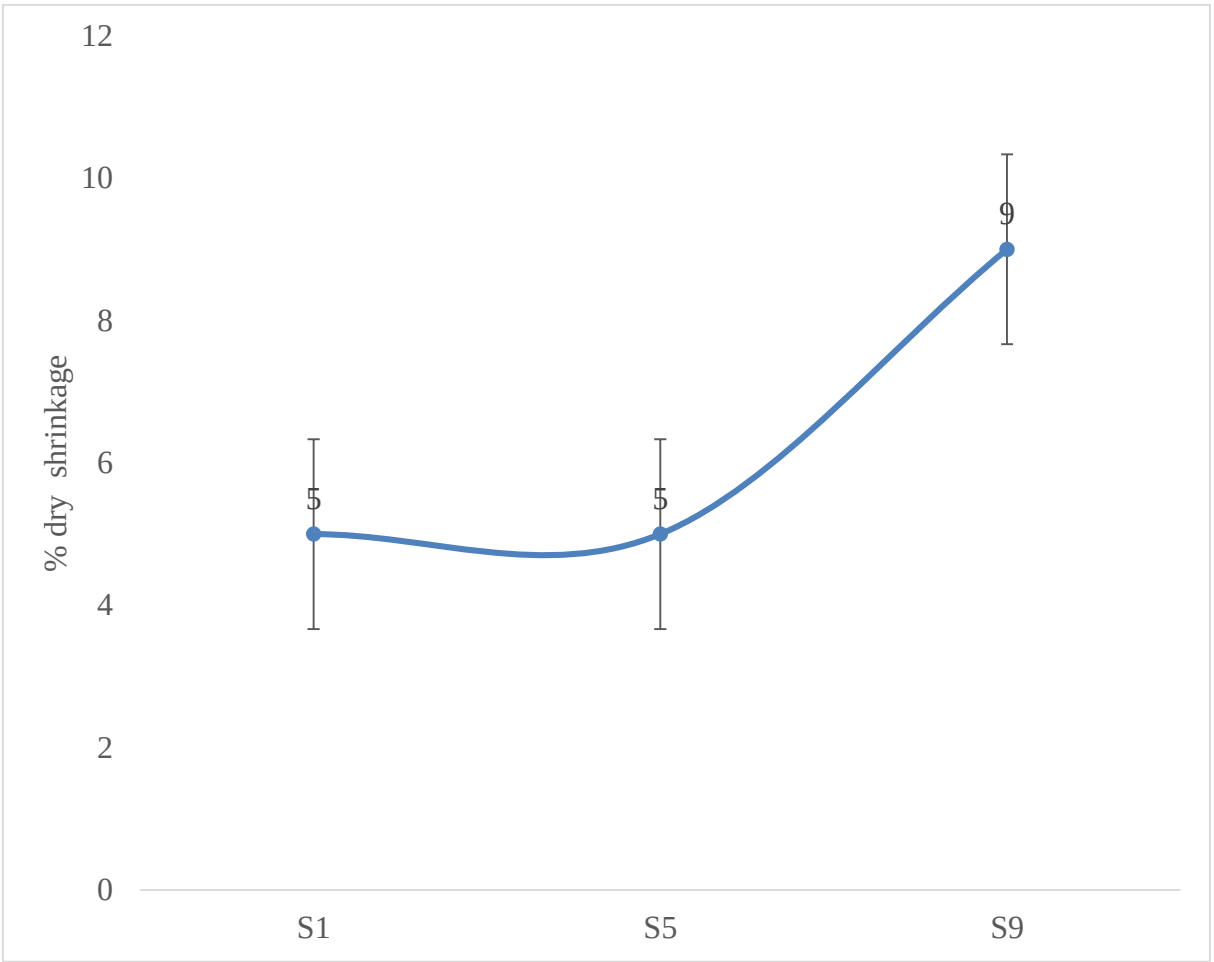

Figure 20: kaolin-zircon % dry shrinkage

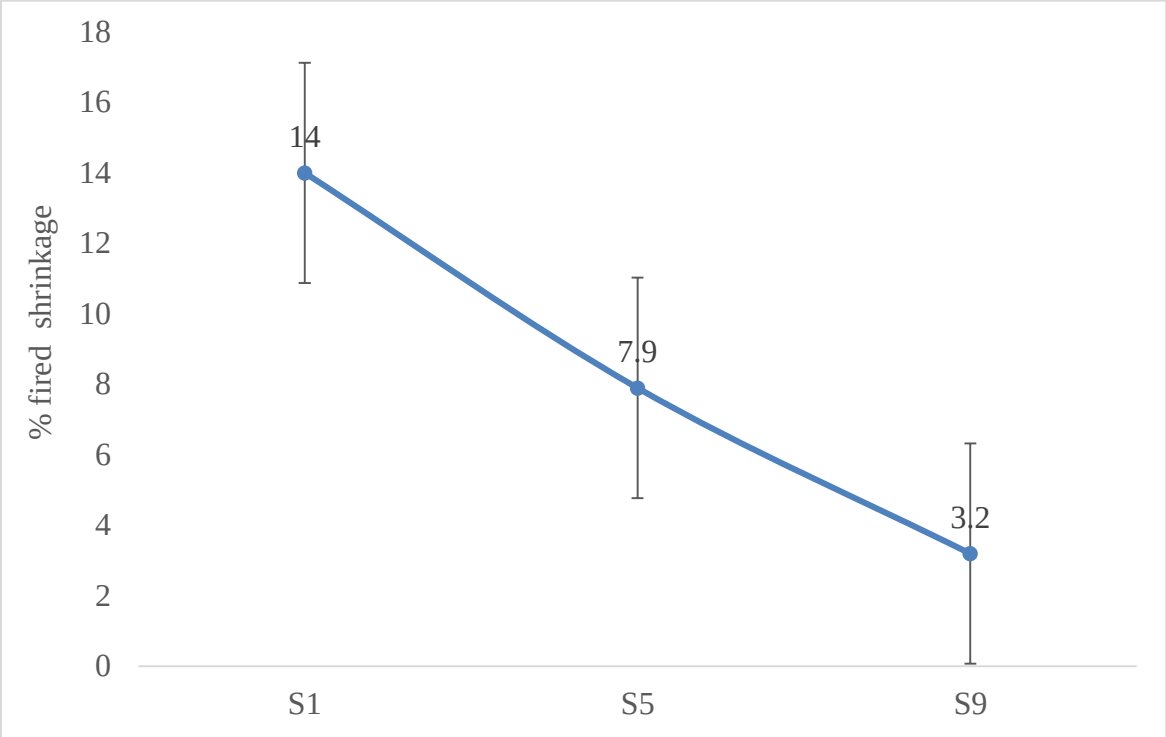

Figure 21: kaolin-zircon % fired shrinkage

An increase in the value of firing shrinkage, as shown in Fig.21 when the ZrO_2 content was 10%, can be interpreted based on the fact that at this content, the better grain distribution allowed the largest area of contact between the grains (i.e., high surface area). The firing shrinking of the kaolin-zircon composite with 50% zircon (ZrO_2) had a slight reduction in sample dimensions due to the increase of the grain size of the compacted sample and the decrease of the contact area between the grains. The increase in firing shrinkage refers to a more efficient firing process due to a homogenous grain distribution and an increase of the contact area between the grains. Moreover, the high rate of contraction affects other properties such as the thermal expansion and thermal shock resistance of the kaolin-zirconia composite sample (Hernández, et. al. 2019).

Corrosion Resistance test

Many different methods have been used to attempt to simulate the environment a refractory is exposed to during commercial service. Each has benefits and limitations and they can be categorized as either static where there is no attempt to simulate motion of the corroding fluid or dynamic where the fluid moves relative to the refractory. These tests are shown schematically in Figure 22. In all of them changes will occur in the slag during the test due to different oxidation states (especially Fe), preferential penetration of specific elements into the brick and dissolution of brick into the slag. These tests are essentially comparative but as discussed by Lee and Zhang [1] still useful for assessing the corrosion mechanisms. All of the static tests suffer from the drawback of the corroding medium (usually slag) rapidly becoming saturated with products of reaction with the solid: a scenario unlikely when slag is moving relative to the refractory and being refreshed with slag free of corrosion products. In the button or sessile drop test (Figure 22a) shaped slag is placed on a refractory substrate, heated to temperature and held for a fixed time to allow the slag to wet and react with the refractory. The sessile drop technique is used to measure interface and surface energies in systems where the liquid is fluid and does not react with the solid but becomes more complicated when reactions occur such as when hot viscous slag is on a refractory solid. In the dipping, immersion or finger test (Figure 22b) one or more cylindrical or square-pillar shaped refractory samples are held in the corrosive slag for a certain period in an electric or induction furnace. In this method the atmosphere is easily controlled and the composition variation of the slag, associated with rapid saturation with reaction products, can be minimized by using a large volume of slag relative to the size of the samples. However, as in the button test no temperature gradient exists in the refractories; they are isothermal i.e. at the same temperature throughout their volume. This

is not the case in commercial practice where a temperature gradient between the hot face of the contact lining and the cold face or safety lining exists. Any slag flow in this test arises from the thermal convection in the slag and so is small. In the crucible, cavity, cup or brick test (Figure 22c) a cored-out refractory brick is filled with slag and exposed to high temperature to promote slag-refractory interaction. This method is popular since it is simple and many samples can be tested in a short time. However, it suffers from the drawbacks associated with static tests i.e. no temperature gradient, rapid saturation of slag composition with reaction products (often all slag is absorbed into the brick) and no slag flow. In the induction furnace test (Figure 22).

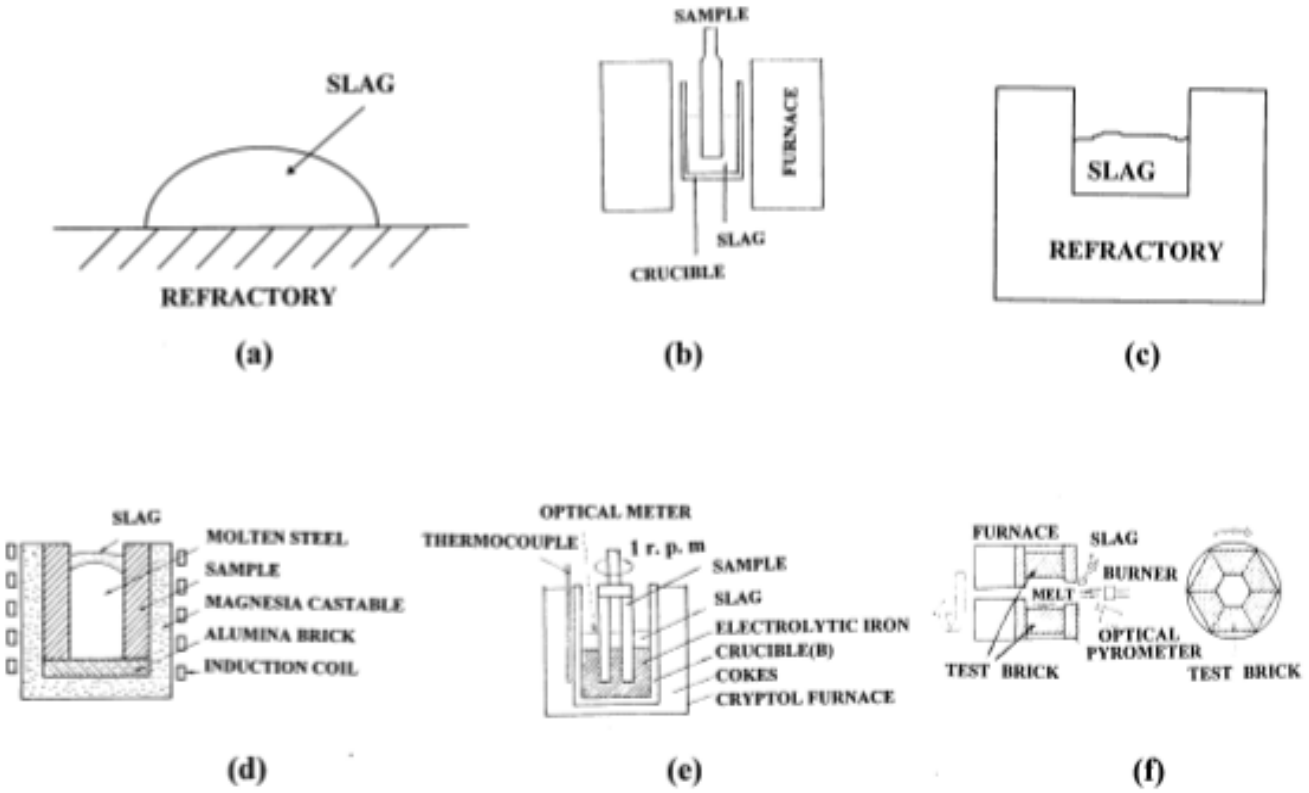

Figure 22: Tests are shown schematically

Isothermal Corrosion Resistance of kaolin-zircon to Molten Glass, C-621

This method compares the corrosion resistance of various refractories to molten glass under static, isothermal conditions. Samples of the kaolin-zircon composite were immersed into molten glass, then heated to a temperature that simulates actual service conditions. The duration of the test was for one hour which is sufficient to produce a glass-line cut of 20–60% of the original sample thickness. After the test, samples are cut in half lengthwise and the width or diameter is measured at the glass line and halfway between the glass line and the bottom of the sample before testing.

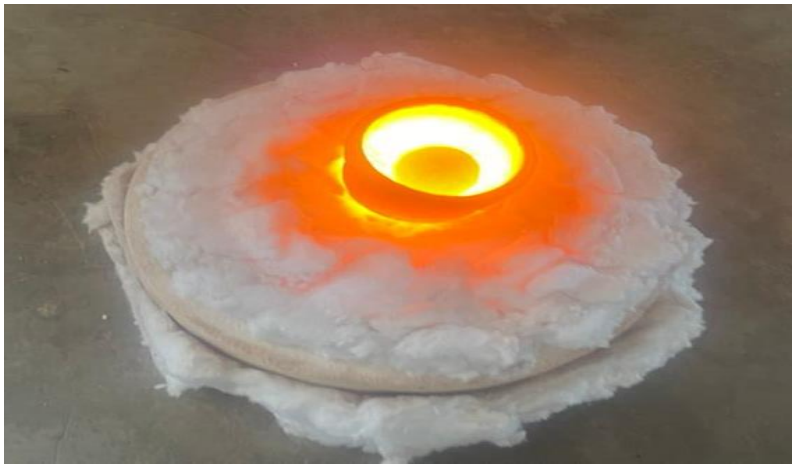

Plate 1: Testing for Corrosion Resistance of kaolin-zircon composite in molten glass

Plate 2: Removal of kaolin-zircon composite from molten glass

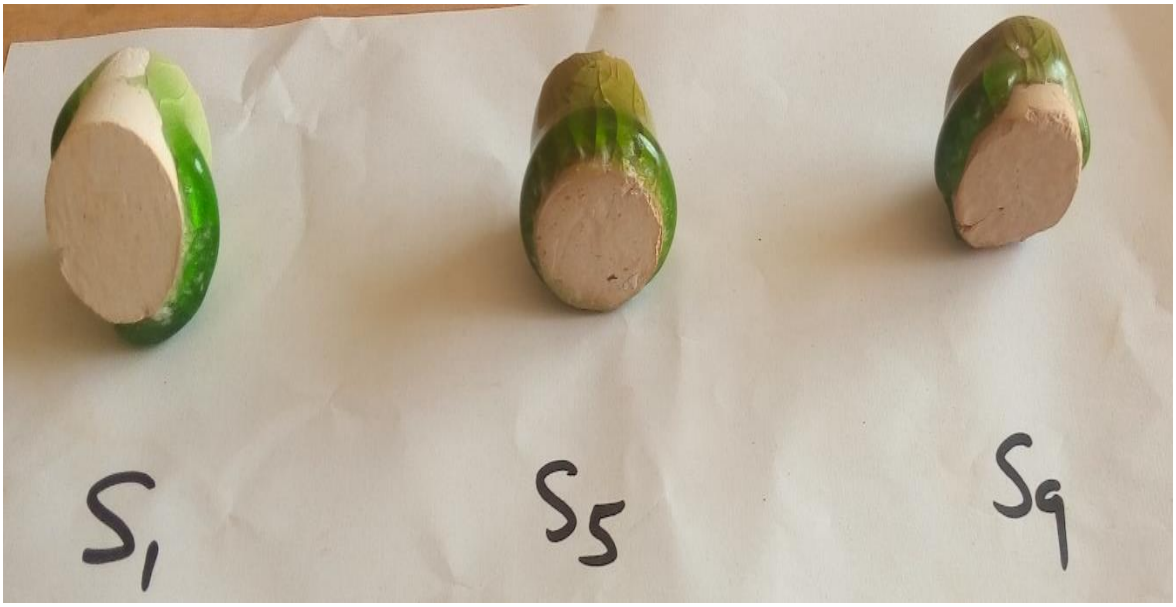

Plate 3: Observing corrosion tendencies on samples of kaolin-zircon composite immersed in molten glass

Corrosion Result

The attack of zircon by soda-lime-silicate glasses is similar to that of AZS materials in that an interface of zirconia crystals embedded in a highly viscous glass is formed. The difference is the lack of alumina, which keeps nepheline from forming and the viscous glass is now a siliceous glass as opposed to an alumina-rich glass which was the case of samples S_1 and S_2 respectively. (Thomas and Brock, 1974) reported that as the sodium content of the attacking glass decreased, the thickness of the zirconia layer decreased. The attack of zircon by a borosilicate glass that contains only about 0.5% Na_2O exhibited no observable alteration. Zircon has been successfully used in contact with high-temperature lithium-alumino-silicate glasses. Kaolin-zircon composite samples S_1 and S_2 showed good resistance, a protective layer of zircon crystals suspended in a very viscous glass is formed by the leaching of silica from the zircon.

Environmentally enhanced strength loss may arise through the following phenomena:

1. Cracking of the surface alteration layers due to excessive mismatch in thermal expansion between the surface and the bulk
2. Melting of secondary phases at high temperature
3. Lowering of the viscosity of a glassy grain boundary phase at high temperature
4. Surface cracking caused by polymorphic transitions in the crystalline phases at the surface
5. Alteration that forms low strength phases
6. Formation of voids and pits, especially true for corrosion by oxidation
7. Crack growth

CONCLUSIUON

The incorporation of fine zircon particles in a relatively finely-grained kaolin-zircon composite reduces the rate of corrosion. The extents of glass penetration and subsequent corrosion rate, decrease significantly with increasing zircon content and associated decreasing accessible porosity. The bulk density was enhanced by increasing the content of zirconia; the glassy silica phase filled the pores and increased the densification of the composite materials that reduced the composite porosity. The zirconia particles improved the mechanical properties due to the phase transformation of the partially stabilized zirconia. The microhardness increased with the increase of zirconia from 10, 50 and 90 wt%; the hardness values were 79.8HV, 87.3HV and 91.2HV respectively.

Zircon additions may be particularly effective in providing a physical barrier to glass penetration into the composite because of the lower solubility of zircon in the molten glass, and local increase in glass viscosity through incorporation of silica.

REFERENCE

A.N. Saud, M.A. Aswad, M.A.A. Al-Dujaili, J. Eng. Appl. Sci. **13**, 22 (2018) 9558.

Afshar, S.; Allaire, C. The Corrosion Kinetics of Refractory by Molten Aluminium. JOM **2000**, 43–46. 1991.

Anseau M. R., Leblud C., Cambier F.: Journal of Materials Science Letters. *2*, 366 (1983).

Beerkens R. G. C., Verheijen O. S.: Physics and Chemistry of Glasses - European Journal of Glass Science and Technology Part *B 46*, 583 (2005).

C. Aksel: Ceramics International Vol. 29(3) (2003), p. 305.

C. Aksel: Materials Letters Vol. 57(4) (2002), p. 992.

Chesters J. H.: *Refractories: Production and Properties*, The Iron and Steel Institute, London 1973.

Ciullo, P.A. (1996) Industrial Minerals and Their Uses: A Handbook and Formulary. Noyes Publications, Westwood, New Jersey.

Claussen N., Jahn J.: J. Am. Ceram. Soc. *63*, 228 (1980).

Davies T. J., Emblem H. G., Sargeant G. K. in: Euro Ceramics II Proceeding of Second European Ceramic Society Conference, p.2587-2591, Ed. Ziegler G. and Hausner H.,

Emblem H. G., Davies T. J, Harabi A., Sargeant G. K. in: XXXV. International Colloquium on Refractories, p.170- 174, 1-2 Oct, Aachen-Germany 1992

Evans G., Baxendale S., Deighton A.: British Ceramic Transaction *100*, 43 (2001).

Evans G., Baxendale S.: British Ceramic Transaction *100*, 90 (2001). holding furnaces. Int. J. Metall. Eng. **2013**, 1, 117–121.

Kashcheev I. D., Mamykin P. S., Bartushka M.: Refractories and Industrial Ceramics *16*, 702 (1975).

Kennedy C. R.: Journal of Materials for Energy Systems *3*, 27 (1981).

Koyama T., Hasayhi S., Yasumori A., Okada K.: Journal of the European Ceramic Society *14*, 295 (1994).

Lathabai S., Hay D. G., Wagner F., Clausen N.: J. Am. Ceram. Soc. *79*, 248 (1996).

Lee, W.E.; Zhang, S. Melt corrosion of oxide and oxide–carbon refractories. Int. Mater. Rev. **1999**, 44, 77–104.

M.F. Hernández, P.V. López, A. Violini, G. Suárez, M.S. Conconi, N.M. Rendtorff, Sci. Sinter. **51** (2019) 51.

Mazdiyasni K. S., Brown L. M.: J. Am. Ceram. Soc. *55*, 548 (1972).

Montanaro L., Perrot C., Negro A.: J. Am. Ceram. Soc. *83*, 189 (2000).

Moore R.E., Skoog A.J.: Ceramic Bulletin. 67, 1180 (1988).

Murray, H.H (2007) Applied clay mineralogy, occurrences, processing and application of kaolins, bentonites, palygorskite-sepiolite, and common clays. Developments in Clay Science, 2, Elsevier, Amsterdam.

Murray, H.H. (2000) Traditional and new applications for kaolin, smectite, and palygorskite: a general overview. Applied Clay Science, 17, 207–221.

Nandy, R.N.; Jogai, R.K. Selection of proper refractory materials for energy saving in aluminium melting and

Pick A. N. in: International Symposium on Refractories p.299-303 Hangzhou-China, November 15-18, 1988.

Prochazka S., Wallace J. S., Claussen N.: J. Am. Ceram. Soc. *66*, 125 (1983).

Rezaie H.R., Rainforth W.M., Lee W.E.: British Ceramic Transactions. 96, 181 (1997).

S. Lathabai, D.G. Hay, F. Wagner and N. Claussen: J. Am. Ceram. Soc., Vol. 79(1) (1996), p. 248.

Schneider H., Okada K., Pask J.: *Mullite and*

Mullite Ceramics, Wiley, London 1994.
Schneider H., Schreuer J., Hildmann B.: Journal of the European Ceramic Society *28*, 329 (2008).

Tamari N., Kondoh I., Tanaka T., Katsuki H.: J. Ceram. Soc. Jpn. 101, 721 (1993).

Thomas, E.A.; Brock, W.W. A post-mortem examination of zircon and bonded alumina-zirconia-silica paving. Proc. 10th International Congress on Glass, Ceram. Soc. Japan, No.2 Refractories and Furnaces, 2–9 to 2–19, 9 July 1974.

Zhao S., Huang Y., Wang C., Huang X., Guo J.: Materials Letter. *57*, 1716 (2003).

J. Xiao, W. Chen, L. Wei, W. He, H. Guo, Materials **13** (2020) 671.

Lathabai S., Hay D. G., Wagner F., Clausen N.: J. Am. Ceram. Soc. *79*, 248 (1996).

Koyama T., Hasayhi S., Yasumori A., Okada K.: Journal of the European Ceramic Society *14*, 295 (1994).

Prochazka S., Wallace J. S., Claussen N.: J. Am. Ceram. Soc. *66*, 125 (1983).

Anseau M. R., Leblud C., Cambier F.: Journal of Materials Science Letters. *2*, 366 (1983).

Claussen N., Jahn J.: J. Am. Ceram. Soc. *63*, 228 (1980).

Zhao S., Huang Y., Wang C., Huang X., Guo J.: Materials Letter. *57*, 1716 (2003).